

From Trace to Pure: Pilot-Scale Scandium Recovery from TiO₂ Acid Waste

Sebastian Hedwig^{a,b,†}, Bengi Yagmurlu^{c,†}, Edward Michael Peters^d, Victor Misev^a, Dirk Hengevoss^a, Carsten Dittrich^d, Kerstin Forsberg^e, Edwin C. Constable^b, Markus Lenz^{a,f*}

^a FHNW, Institute for Ecopreneurship, Hofackerstrasse 30, 4132, Muttenz, Switzerland

^b University of Basel, Department of Chemistry, Mattenstrasse 24a, 4058, Basel, Switzerland

^c TU Clausthal, Institute of Mineral and Waste Processing, Recycling and Circular Economy Systems, Walter-Nernst-Str. 9, 38678, Clausthal-Zellerfeld, Germany

^d MEAB Chemie Technik GmbH, 52068 Aachen, Germany

^e KTH Royal Institute of Technology, Department of Chemical Engineering, 100-44 Stockholm, Sweden

^f Wageningen University, Department of Environmental Technology, Bornse Weiland 9, 6700 AA, Wageningen, The Netherlands

† S.H. and B.Y. contributed equally to this paper.

* Corresponding author, contact: markus.lenz@fhnw.ch, +41 61 228 5686

Abstract

Scandium (Sc), declared a critical raw material in the European Union (EU), could face further supply issues as the EU depends almost entirely on imports from China, Russia and Ukraine. In this study, a tandem nanofiltration-solvent extraction procedure for Sc recovery from titania (TiO₂) acid waste was piloted and then augmented by antisolvent crystallisation. The new process, comprising advanced filtration (hydroxide precipitation, micro-, ultra- and nanofiltration), solvent extraction and antisolvent crystallisation, was assessed in relation to material and energy inputs and benchmarked on ScF₃ production. From ~1 m³ of European acid waste containing traces of Sc (81 mg L⁻¹), ~13 g Sc (43% yield, nine stages) was recovered as (NH₄)₃ScF₆ with a purity of approximately 95%, demonstrating the technical feasibility of the approach. The production costs per kilogram of ScF₃ were lower than reported market prices, which underscores a competitive process at scale. Although a few technical bottlenecks (e.g. S/L separation and electricity consumption) need to be overcome, combining advanced filtration with solvent extraction and antisolvent crystallisation promises a future supply of this critical raw material from European secondary sources.

Highlights

- First pilot campaign for Sc recovery from European TiO₂ acid waste employing nanofiltration
- Sc (13 g) was extracted and crystallised as (NH₄)₃ScF₆ with high purity (> 95%)
- The process was benchmarked on ScF₃ production, promising a competitive production price even with non-optimised conditions

Keywords

Critical raw material, secondary source TiO₂ pigment production, chloride route, nanofiltration, solvent extraction, antisolvent crystallisation, scandium, cost

1 Introduction

2 Supply chains are the backbone of the economy. However, their resilience is increasingly chal-
3 lenged by social, environmental and geopolitical factors, potentially leading to disruption and,
4 consequently, economic damage. Herein, critical raw materials (CRM) are a key factor, as they
5 are economically important but at risk in supply. To identify and counteract raw material criticality,
6 the European Union (EU) has launched a raw materials initiative, publishing a list of CRMs every
7 three years since 2011.¹ The rare earth metal scandium (Sc) has been included on the list since
8 2017 because of its applications in high-strength aluminium alloys and high-efficiency fuel cells.^{1,2}
9 Used in aircraft engineering, up to 20% lighter airplanes could be built compared with today's
10 standards.³ Sc₂O₃ is vital for commercialised solid oxide fuel cells, which facilitates the direct
11 conversion of hydrogen to electrical power.^{3,4}

12 However, market acceptance has been low due to a severe lack of Sc supply and extremely high
13 prices.⁵ Until recently, the majority of the supply came from China (66%), with Russia (26%) and
14 Ukraine (7%) as other suppliers.⁶

15 The underdevelopment of Sc production can be partially attributed to the scarcity of Sc ores. Sc
16 has a low affinity to common ore-forming anions and, thus, is widely dispersed in the lithosphere.⁷
17 Consequently, Sc recovery from secondary sources, where it is concentrated, is a compelling
18 notion. One example of secondary sources is waste from the chloride route for white pigment
19 (TiO₂) production. This two-stage process is responsible for 3–4 Mt a⁻¹ or approx. 50% of the
20 global TiO₂ supply.⁸ Rutile or titania-rich starting materials are converted into volatile TiCl₄ using
21 Cl₂ and coke. After separation, TiCl₄ reacts with O₂ and pure TiO₂ is obtained, whereas Cl₂ is
22 recycled. Impurities accompanying the starting materials are washed out in the scrubber water.⁹
23 These impurities contain HCl (approx. 15%), unreacted ore, coke, and a variety of metal chlorides.
24 Sc has been reported to be present in the range of several hundred ppm.^{9,10}

25 Some approaches have been developed to recover Sc. Conventionally, solvent extraction (SX) is
26 used, followed by precipitation as a hydroxide or oxalate salt.^{11,12} After calcination at temperatures
27 in the range of 700–800 °C, Sc₂O₃ is obtained.¹³ The oxide is then converted to ScF₃ using hy-
28 drofluoric acid.¹⁴ Afterwards, metallothermic reduction of ScF₃ is conducted to produce Sc metal
29 or Al-Sc alloys.^{14–16}

30 Remmen et al. presented nanofiltration (NF) using tailor-made layer-by-layer assembled mem-
31 branes (LbL membranes) as a viable option, retaining most of the Sc while partially depleting
32 impurities.³

33 We showed in our previous study that the combination of NF and SX can be successfully utilised
34 to produce a strip liquor containing > 97% pure (NH₄)₃ScF₆ from genuine TiO₂ acid waste.¹⁰ Peters
35 et al. reported the further purification of such Sc strip liquors using antisolvent crystallisation (ASC)
36 with ethanol to yield > 98.7% pure (NH₄)₃ScF₆.¹⁷ It was also reported that the metals are usually

37 present in the solid product in relative proportions that reflect their abundance in the strip liquor.¹⁸
38 Furthermore, studies on the solubility of $(\text{NH}_4)_3\text{ScF}_6$ in NH_4F solutions and NH_4F -alcohol mixtures
39 were published.¹⁹ The ammonium metal fluorides of Fe and Al were shown to exhibit considerably
40 lower solubilities than $(\text{NH}_4)_3\text{ScF}_6$, while $(\text{NH}_4)_3\text{ZrF}_7$ exhibited comparable solubility to $(\text{NH}_4)_3\text{ScF}_6$,
41 in NH_4F -alcohol mixtures.¹⁸ Further studies showed the importance of supersaturation control on
42 the quality of the product crystals and that trade-off exists between product quality and productiv-
43 ity.²⁰
44 However, a discrepancy was found between the dimensions of the prospected Sc recovery route
45 and the volume of waste generated. Therefore, this study aimed to upscale the previously pre-
46 sented seven-stage NF-SX process by treating $\sim 1 \text{ m}^3$ of real TiO_2 acid waste. In addition, the final
47 solid product was synthesised, and the quality was enhanced by ASC. The newly developed pro-
48 cedure was assessed in terms of the material and energy costs required to produce 1 kg ScF_3 as
49 the closest marketable product in the Sc supply chain.

50

51 **Materials and Methods**

52 **Chemicals and materials**

53 Acid waste was obtained from a TiO_2 producer in the Netherlands. NaOH solution (30% w/w) for
54 pH adjustment was provided by Getec Park.Swiss, Switzerland.

55 HCl (37% w/w, laboratory grade, PANREAC QUIMICA S.L.U., Spain), NH_4F (reagent grade,
56 Merck, Germany), D2EHPA (Lanxess, Germany), N1923 (HalloChem, China) and dearomatised
57 kerosene (Exxsol D80, ExxonMobile, Germany) were used for SX.

58 Analytical-grade ethanol (99.95% v/v) for the ASC experiments was purchased from VWR, Swe-
59 den.

60 **Analytical methods**

61 **Triple quadrupole inductively coupled plasma mass spectrometry (QqQ-ICP-MS)**

62 Samples were diluted using nitric acid (3% w/w) and an autodilution system (Simprep, Teledyne
63 Cetac Technologies, USA). Thereafter, they were analysed using QqQ-ICP-MS. The analysis was
64 performed on an 8800 QqQ-ICP-MS system (Agilent, Switzerland) using general-purpose opera-
65 tional settings. Quantification was performed via multi-element standards (0-50 ppb, seven
66 points). To account for matrix effects, ^{103}Rh was used as the internal standard. To quantify $^{23}\text{Na}^+$,
67 $^{52}\text{Cr}^+$, $^{55}\text{Mn}^+$, $^{56}\text{Fe}^+$, $^{60}\text{Ni}^+$, $^{66}\text{Zn}^+$, $^{89}\text{Y}^+$, $^{137}\text{Ba}^+$, $^{139}\text{La}^+$, $^{140}\text{Ce}^+$, $^{141}\text{Pr}^+$, $^{146}\text{Nd}^+$, $^{147}\text{Sm}^+$, $^{153}\text{Eu}^+$, $^{157}\text{Gd}^+$,
68 $^{159}\text{Tb}^+$, $^{163}\text{Dy}^+$, $^{165}\text{Ho}^+$, $^{166}\text{Er}^+$, $^{169}\text{Tm}^+$, $^{172}\text{Yb}^+$, $^{208}\text{Pb}^+$, ^{232}Th , and $^{238}\text{U}^+$, the ICP-MS was operated in
69 single-quad mode using helium as collision gas. Meanwhile, $^{24}\text{Mg}^+$, $^{27}\text{Al}^+$, $^{39}\text{K}^+$, $^{45}\text{Sc}^+$, $^{47}\text{Ti}^+$, $^{51}\text{V}^+$

70 and $^{90}\text{Zr}^+$ were measured in triple-quad mass-shift mode using O_2 as a reaction gas. $^7\text{Li}^+$ concen-
71 tration was determined using no-gas single-quad mode.

72 **Inductively coupled plasma optical emission spectrometry (ICP-OES)**

73 Element concentrations in the ASC tests were analysed by ICP-OES (iCAP 7400, Thermo Fisher
74 Scientific Inc., USA). Supernatant samples were withdrawn and filtered (0.2 μm , polypropylene
75 syringe filters) prior to dilution. HNO_3 (3.45% v/v) was used for dilution.

76 **Powder X-ray diffraction (XRD) and scanning electron microscopy (SEM)**

77 Powder XRD spectra were recorded on a Siemens D5000 (Siemens AG, Germany) to examine
78 the crystalline phases of the product. Micrographs were captured via SEM using a Philips/FEI-XL
79 30 series environmental scanning electron microscope (Philips, The Netherlands) to assess crys-
80 tal size and morphology.

81 **Neutralisation**

82 An intermediate bulk container (IBC, 1 m^3 volume) was equipped with an agitator (SR6, Simix,
83 Germany) and NaOH dosing pumps (Vantage 5000, Verder, Germany). An exhaust air connec-
84 tion (Figure S1) was used for pH adjustment. The pH and temperature were measured using an
85 inline sensor (Aquastick, Thermo Fisher Scientific Inc., The Netherlands). Caustic soda (30% w/w,
86 150 L) was successively added to the acid waste (800 L) under stirring until pH 1.5 was reached.
87 The reaction mixture (950 L) was stirred for 24 h before settling for 48 h.

88 **Microfiltration (MF)**

89 MF was carried out using a bag filtration unit (2-EF6-F, Eurowater, Germany; Figure S1) with two
90 filtration bags (size 2, polypropylene, 1 μm nominal removal rate, 17 L volume). The filtration unit
91 was fed by emptying the precipitation tank from top to bottom using a dip tube and a peristaltic
92 pump (Vantage 5000, Verder, Germany) with a variable flow rate until the pressure reached 2 bar.
93 Afterwards, pressurised air (4 bar) was applied to further dewater the filter cake. The filter bags
94 were emptied periodically (after 8, 15, 20 and 23 h) and reused until the filtration of the batch was
95 completed. In total, 700 L filtrate was separated from 250 L hydroxide sludge.

96 **Ultrafiltration (UF) and NF**

97 Both UF and NF were carried out in cross-flow operation mode using a modified filtration system
98 (Osmo Inspector, Convergence, The Netherlands; Figure S1). For UF, 1812 spiral wound ele-
99 ments (UP150, Microdyn-Nadir, Germany, membrane area: 0.23 m^2 , MWCO: 150 kDa) were
100 used. For batch UF (500 L), a transmembrane pressure (TMP) of 5–20 bar was applied at a cross-
101 flow rate of 8 L min^{-1} and T of 25 $^\circ\text{C}$. The UF was stopped after 80% permeate recovery (400 L).

102 A 2540 spiral wound element (NanoPro A-3014, AMS Technologies, Israel; membrane area: 1.6
103 m², MWCO: 400 Da) was used for NF. Prior to use, the module was compacted overnight by
104 filtrating water (TMP: 15 bar, cross-flow rate: 8 L min⁻¹, T: 25 °C). NF was operated in batch mode,
105 aiming for a permeate recovery of 60%. The TMP was kept constant at 35 bar at a cross-flow rate
106 of 8 L min⁻¹. In total, 250 L was filtrated in five batches (50 L each) using the same membrane
107 module without intermediate washing (Figure 3). Approximately 100 L of dark green concentrate
108 was obtained after NF. Equations for calculating the concentration factor (X), element (M) reten-
109 tion (R_M), permeate flux (J_{permeate}) and specific energy consumption (SEC) are given in SI.

110 Solvent extraction

111 SX was conducted with NF concentrate (100 L) in continuous counter-current operation using 12
112 PVDF MEAB MSU-0.5 mixer-settler units (MEAB Chemie Technik GmbH, Germany) connected
113 in series (Figure S2). The active mixer volume of the MSU-0.5 was 0.12 L, while the settler volume
114 was 0.48 L with a loading surface area of 0.006 m². The number of stages in each process step
115 (extraction, scrubbing and stripping) was determined by constructing the McCabe-Thiele diagrams.
116 Therefore, the respective solutions in each step were contacted with the organic solution with
117 different phase ratios to obtain the equilibrium loading, scrubbing and stripping curves (Figure 4).
118 To minimise Fe co-extraction, Fe⁰ (1.5 g per litre) was added to the NF concentrate in a separate
119 tank, reducing any Fe³⁺ to Fe²⁺. Afterwards, Sc was extracted using 0.2 mol·L⁻¹ D2EHPA with
120 0.05 mol L⁻¹ N1923 in D80 kerosene with a phase ratio of 4 (aqueous:organic). Co-extracted
121 impurities in the loaded organic were scrubbed with HCl (4 mol L⁻¹) with a phase ratio of 0.1. The
122 scrub liquor was recycled into the SX feed solution to eliminate Sc losses and control the pH for
123 better Sc selectivity during SX. To remove entrained acid in the organic phase, which could lead
124 to HF formation during stripping with NH₄F, scrubbed organic was washed with NaCl solution (2%
125 w/w) with a phase ratio of 0.1. For Sc stripping, NH₄F solution (3 mol L⁻¹) was added to the washed
126 organic with a phase ratio of 0.33, yielding an (NH₄)₃ScF₆ solution. Finally, the organic was made
127 to come in contact with HCl (2 mol L⁻¹) with a 0.1 phase ratio to recondition the stripped organic
128 phase and neutralise deprotonated D2EHPA.

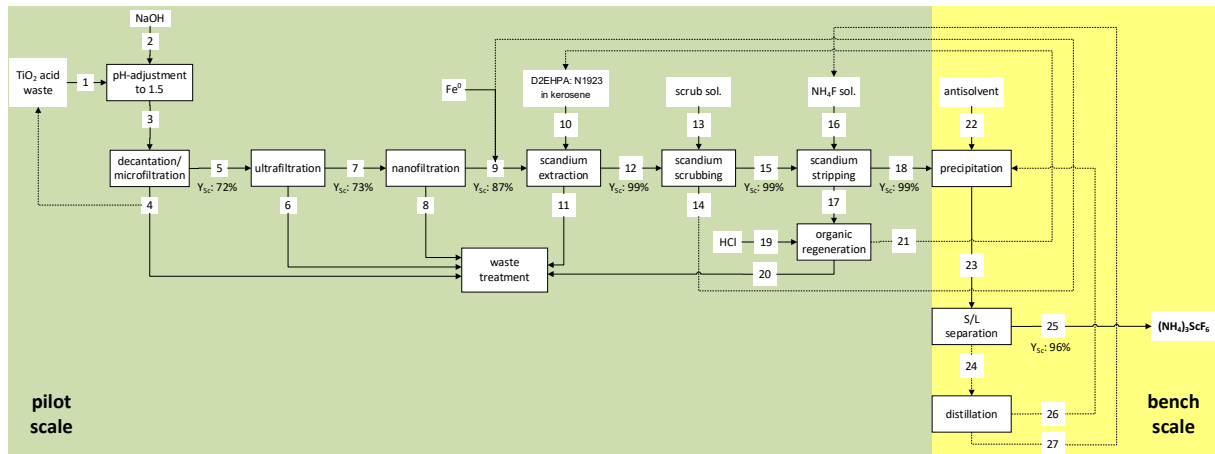
129 Antisolvent crystallisation

130 A strip liquor (pH= 5.74) after SX and stripping with NH₄F solution (3 mol L⁻¹) was used for the
131 ASC tests. All tests were conducted in triplicate. To examine the Sc precipitation efficiency, eth-
132 anol (99.95%) was added all at once to aliquots of the strip liquor to reach final concentrations of
133 2, 4, 6, and 8 mol L⁻¹, which corresponded to ethanol:strip liquor volumetric ratios of approximately
134 0.13, 0.31, 0.54, and 0.88, respectively. In addition, the precipitation efficiency of the other ele-
135 ments was examined at an ethanol concentration of 8 mol L⁻¹. After ethanol addition, all suspen-
136 sions were agitated at 500 rpm using a magnetic stirrer under ambient conditions for 1 h. The

137 solid material obtained after crystallisation at 8 mol L⁻¹ ethanol concentration was dried overnight
138 under ambient conditions and used for further analysis.

139 Results and Discussion

140 Process flow scheme



141
142 **Figure 1:** Block flow diagram of the scandium recovery process.

143 The process (Figure 1) was based on previous studies and comprised nine stages, excluding
144 organic regeneration and final waste treatment.^{10,17} The first four stages (pH adjustment to NF)
145 are summarised under the term 'advanced filtration' (AF). Stages five to seven (Sc extraction,
146 scrubbing and stripping) are named SX. The last two stages (precipitation and S/L separation)
147 are summarised under ASC. While AF and SX were tested on a pilot scale, ASC was conducted
148 on a bench scale to optimise the parameters for recovering Sc from the strip liquor (Figure 1).

149
150

Table 1: Mass balance of the Sc recovery process based on 100L of NF concentrate. Stream numbers refer to the steps defined previously (details in Figure 1), with the key streams being the acid waste (1), the NF concentrate (9), the SX raffinate (11), the strip liquor (18) and the crystallised $(\text{NH}_4)_3\text{ScF}_6$ product (25).

Process step	pH-adjustment			Microfiltration		Ultrafiltration		Nanofiltration		Sc extraction			Sc scrubbing			Sc stripping			Precipitation & S/L Separation		
	1	2	3	4	5	6	7	8	9	10	11	12	13	14	15	16	17	18	24	25	
Volume [L]	357	67	424	112	313	63	250	150	100	25	100	25	2.5	2.5	25	10	25	10	10	0.01	
Sc	Amount [g]	29 ± 1	-	-	8.5 ± 0.2	21 ± 1	6.1 ± 0.3	15 ± 1	1.9 ± 0.3	13.0 ± 0.4	-	0.10 ± 0.01	13 ± 1	-	0.005 ± 0.001	13 ± 1	-	0.10 ± 0.01	12.7 ± 0.4	0.500 ± 0.002	12.6 ± 0.16
	Yield* [-]	-	-	-	0.29	0.72	0.29	0.73	0.13	0.89	-	0.01	1.00	-	0.00	1.00	0.00	0.01	0.98	0.04	0.96
Ti	Amount [g]	1900 ± 50			1600 ± 50	200 ± 10	200 ± 10	1.1 ± 0.1	0.4 ± 0.1	0.6 ± 0.1	-	0.4 ± 0.1	0.03 ± 0.01	-	0.006 ± 0.001	0.020 ± 0.002	-	n.d.	0.1 ± 0.1	0.110 ± 0.003	0.00 ± 0.01
	Yield* [-]	-	-	-	0.89	0.11	>0.99	0.01	0.32	0.58	-	0.67	0.05	-	0.20	0.67	0.00	0.00	5.00	1.00	0.00
Fe	Amount [g]	11300 ± 300			2100 ± 100	9000 ± 500	1700 ± 50	6300 ± 100	3500 ± 200	2900 ± 100	-	2200 ± 200	64 ± 9	-	n.d.	1.4 ± 0.3	-	n.d.	0.17 ± 0.05	0.110 ± 0.001	0.02 ± 0.01
	Yield* [-]	-	-	-	0.19	0.81	0.29	0.7	0.55	0.46	-	0.76	0.02	-	0.00	0.02	0.00	0.00	0.12	0.85	0.15
Zr	Amount [g]	720 ± 30			740 ± 30	100 ± 5	89 ± 4	0.11 ± 0.01	0	0.11 ± 0.01	-	0.01 ± 0.01	0.12 ± 0.03	-	0.02 ± 0.01	0.11 ± 0.01	-	0.02 ± 0.01	0.09 ± 0.04	0.020 ± 0.001	0.080 ± 0.003
	Yield* [-]	-	-	-	0.88	0.12	>0.99	0.001	0	100	-	0.09	1.09	-	0.17	0.92	0.00	0.18	0.82	0.20	0.80
Th	Amount [g]	41 ± 1			39 ± 4	8 ± 1	5 ± 1	2 ± 1	0.03 ± 0.01	1.9 ± 0.2	-	0.2 ± 0.03	1.7 ± 0.4	-	0.05 ± 0.03	1.8 ± 0.5	-	0.2 ± 0.1	0.4 ± 0.1	0.020 ± 0.001	0.210 ± 0.006
	Yield* [-]	-	-	-	0.83	0.17	0.78	0.22	0.01	1.07	-	0.11	0.89	-	0.03	1.06	0.00	0.11	0.22	0.09	0.91
U	Amount [g]	9.3 ± 0.2			9 ± 1	1.2 ± 0.2	1.9 ± 0.2	0.97 ± 0.03	0.71 ± 0.02	0.24 ± 0.01	-	n.d.	0.20 ± 0.05	-	0.02 ± 0.01	0.19 ± 0.04	-	n.d.	0.18 ± 0.03	0.080 ± 0.005	0.150 ± 0.007
	Yield* [-]	-	-	-	0.88	0.12	0.22	0.78	0.73	0.24	-	0.00	0.83	-	0.10	0.95	0.00	0.00	0.95	0.36	0.64
V	Amount [g]	725 ± 8	-	-	160 ± 10	520 ± 20	110 ± 2	368 ± 7	193 ± 9	178 ± 5	-	140 ± 10	10 ± 2	-	9 ± 2	1.1 ± 0.3	-	0.3 ± 0.1	0.6 ± 0.1	0.280 ± 0.003	0.32 ± 0.01
	Yield* [-]	-	-	-	0.22	0.72	0.21	0.71	0.53	0.48	-	0.79	0.06	-	0.90	0.11	0.00	0.27	0.55	0.47	0.53
Al	Amount [g]	1710 ± 70			480 ± 60	1410 ± 70	280 ± 10	910 ± 40	192 ± 7	900 ± 40	-	710 ± 20	22 ± 3	-	21 ± 2	0.3 ± 0.1	-	0.2 ± 0.1	0.09 ± 0.02	0.40 ± 0.02	0.10 ± 0.05
	Yield* [-]	-	-	-	0.28	0.82	0.20	0.64	0.21	0.99	-	0.79	0.02	-	0.95	0.01	0.00	0.67	0.30	0.80	0.20

* Yield per stage was calculated based on inputs from the direct upstream.

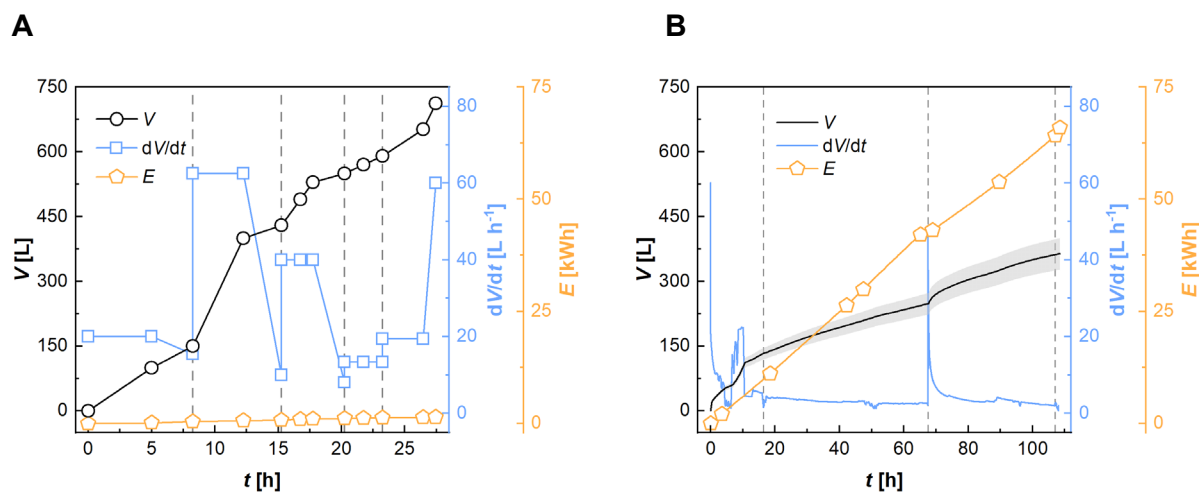
151

152 From the acid waste (stream 1), 12.6 g of Sc (43%) was recovered in the form of $(\text{NH}_4)_3\text{ScF}_6$
 153 (stream 25; Table 1). The total recovery yield after nine stages was higher than previously re-
 154 ported for bench scale tests (36%, six stages)¹⁰, but still comparably lower than reported in other
 155 studies, such as Zhou et al. (68.6%)²¹, Chen et al. (90.34%)²², Zhou et al. (95%)^{23,24}. Major losses
 156 occurred in the early stages of AF (streams 1 to 9) within this study. Approximately half of the Sc
 157 (~14.6 g) was lost after pH adjustment, MF and UF (streams 1 to 7). In contrast, virtually no losses
 158 occurred during SX (streams 9 to 18) and just minute amounts of Sc were lost (0.4 g, 3%) during
 159 ASC (streams 18 to 25). Therefore, considering the stages from NF to ASC, ~84% yield was
 160 achieved (six stages, streams 7 to 25). Moreover, with respect to the latest five stages only (SX
 161 to ASC, streams 9 to 25), ~97% Sc yield was reached. Thus, while the yield of MF and UF leaves
 162 room for improvement, the yield of the other process stages was on par with the aforementioned
 163 studies.

164

165 Advanced filtration

166 Precipitation and removal of interfering metals



167 **Figure 2:** Volume of filtrate generated, flow rate and energy consumption during microfiltration (A) and ultrafiltration (B). The grey
 168 dashed lines indicate the exchange of filter bags/ultrafiltration membranes.

169 The received TiO_2 acid waste contained Sc (~81 mg L⁻¹) and more than 30 other elements up to
 170 multiple grams per litre (Table 1). Some of these elements disturb SX but precipitate at pH 1.5,
 171 while the majority of Sc is preserved in the solution.^{3,10}

172 After pH adjustment and MF, the majority of Sc (72%) remained in the filtrate (stream 5, Table 1).
 173 This result was higher than during the bench scale tests, where only 56% of the Sc was pre-
 174 served.¹⁰ Regarding the impurities, similar to the bench scale tests¹⁰, with the hydroxide sludge
 175 (~250 L, stream 4), interfering elements were effectively removed (Ti: 88%, Zr: 88%, Nb 88%, U:

176 88%, Th: 83%). S/L separation worked slightly better on the pilot scale, yielding 74% filtrate re-
177 covery in comparison to 69% during the bench-scale experiments.¹⁰

178 The ratio between sludge and bag filter volume changed disproportionately during upscaling. In
179 the bench-scale tests, 1 L sludge was removed using a bag filter of 1.9 L volume (ratio of 0.53).¹⁰
180 In the pilot phase, 250 L of sludge (stream 4) was separated using two bag filters of 17 L each
181 (ratio of 7.4). As a result, the bag filters had to be emptied multiple times. The precipitate was
182 allowed to settle for over 48 h, and the reactor was drained from top to bottom to prevent prema-
183 ture filter clogging. This strategy succeeded, as reflected in the initially higher filtration rates and
184 longer operating intervals before the discharge of the filter cake than at the end of filtration (Figure
185 2A). However, the start-up phase (0–8 h) was exceptional, as the pump speed and immersion
186 depth of the dip tube were not optimal, resulting in a low filtration rate and filter clogging after
187 150 L of filtrate was produced (Figure 2A).

188 Only a thickened sludge was obtained with no fully dewatered filter cake after MF. Therefore, the
189 hygroscopic nature of the precipitated hydroxides impeded S/L separation. Flushing with pressur-
190 ised air helped recover more filtrate but did not represent a satisfactory solution for continuous
191 production. A plate filter press could help optimise the filtrate yield through higher compression
192 and ease the procedure through automated discharge of the separated precipitate.²⁵

193 The obtained filtrate was still partially turbid, being especially visible after filter exchange. This
194 could be due to the use of extremely coarse filter bags, whereby the particle removal efficiency is
195 usually low before the build-up of a filter cake. Felt bags with a nominal filter rating of 1 μm were
196 used in this process. This means that particles of 1 μm and larger are retained but to an undefined
197 percentage, as indicated by the manufacturer.^{26,27} For future tests, filtration materials with 1 μm
198 absolute rating (i.e. assured removal rate of > 99% for particulates of $\geq 1 \mu\text{m}$) could achieve a
199 better separation result.

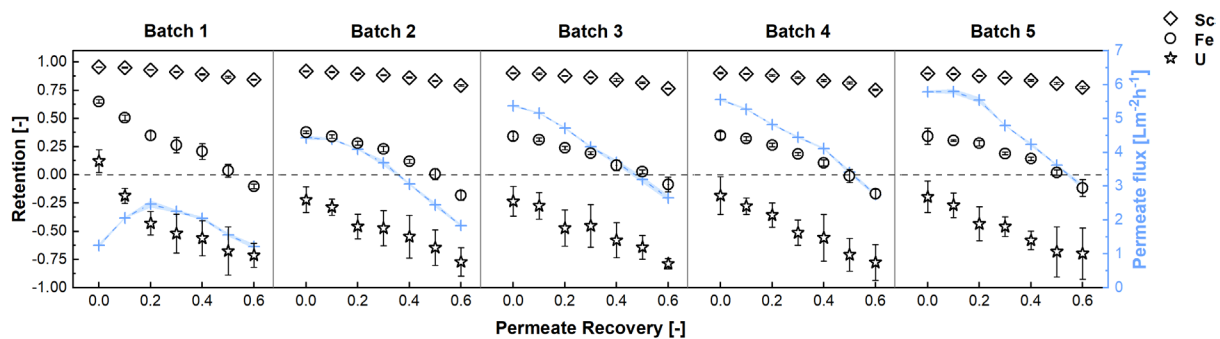
200 SEC for MF was $\sim 2.1 \text{ kWh m}^{-3}$ of filtrate (Figure 2A), similar to the SECs reported for the MF of
201 slurries, such as using a rotating MF (4 kWh m^{-3}).²⁸

202 Following MF, the filtrate was further clarified using UF. In this process, a 0.4 m^3 ultrafiltrate
203 (stream 7) was obtained, containing 73% of the Sc from the 0.5 m^3 MF permeate (stream 5) (Table
204 1, Figure 2B). Multiple elements were effectively removed with the residual suspended particles,
205 including Ti (> 99%), Zr (> 99%), Nb (> 99%) and Th (78%) (Table 1).

206 Directly after the deployment of new spiral wound elements, high filtration rates ($40\text{--}60 \text{ L h}^{-1}/170\text{--}$
207 $260 \text{ L m}^{-2} \text{ h}^{-1}$) were observed during UF. However, these rates decreased to < 10% of their initial
208 value within 5 h of operation. Rinsing with diluted hydrochloric acid did not restore permeability
209 (tested after 16 and 107 h). After $\sim 109 \text{ h}$, 80% permeate recovery was achieved, and UF was
210 stopped because the feed had considerably thickened and the permeate flow had irreversibly
211 decreased to below 2 L h^{-1} .

212 Owing to the low filtration rate (average $3.6 \text{ L h}^{-1}/16 \text{ L m}^{-2} \text{ h}^{-1}$), the SEC for permeate production
 213 was high, eventually reaching 165 kWh m^{-3} . Despite taking the challenging nature of the feed into
 214 account, the SEC appears to be at least an order of magnitude higher than the typical values
 215 reported for UF.^{29,30} Apparently, the spiral wound elements were rapidly clogged, which drastically
 216 affected their performance. Nevertheless, the UF was continued to provide feed for downstream
 217 NF experiments. This approach, however, was not cost-effective. High particle loading in the UF
 218 feed should be avoided through better S/L separation upstream of the UF to improve the opera-
 219 tion. In this regard, employing a filter press (as used at the TiO_2 manufacturing facility) or drum
 220 centrifugation would be recommended.³¹ In addition, different membrane designs could ease
 221 cleanability, allowing the recovery of lost permeability, thereby keeping the filtration rates high
 222 and increasing membrane lifespan. In this process, capillary or tubular membrane elements
 223 should be tested.^{25,32} If the permeate flux is kept in the measured starting range of $170\text{--}260 \text{ L m}^{-2} \text{ h}^{-1}$,
 224 the SEC can be reduced by up to 95%. The suggested changes for MF and UF should result
 225 in higher Sc yields (currently 53%, three stages), thereby boosting the overall process efficiency.

226 NF



227

228 **Figure 3:** Element retentions and permeate fluxes during the five batches (each 50 L) of nanofiltration.

229 The pilot NF was based on bench-scale tests, aiming for 60% permeate recovery (i.e. a final
 230 concentration factor of 2.5 (Equation S1)).¹⁰ The targeted amount of NF concentrate (100 L) was
 231 set to allow downstream pilot SX. Thus, five batches of ultrafiltrate (50 L each) were concentrated
 232 with the same 2540 spiral wound membrane elements.

233 Sc retention during the pilot experiments was similar to that of the bench scale tests.¹⁰ Starting at
 234 0.96, a slight decrease to 0.85 after 2.5-fold concentration was observed in the first batch (Figure
 235 3). Sc retention was slightly lower in batch two, with initial and final values of 0.92 and 0.79,
 236 respectively (Figure 2A). The retention in batches three to five seemed to have reached constant
 237 values, being in each case initially 0.90 and 0.76 after 60% permeate recovery (Figure 3). The
 238 measured Sc retention over the whole NF and all batches combined was 0.90, leading to a total
 239 Sc recovery yield of 87% (stream 9, Table 1), which was slightly higher than that reported for the
 240 bench-scale tests (84%).¹⁰ Overall, the Sc concentration was increased by a factor of ~ 2.2 (from
 241 60 mg L^{-1} to 130 mg L^{-1} ; Table 1).

242 Some impurities were successfully depleted by NF, such as Fe (-55%), V (-53%) or U (-73%)
243 (Table 1). For instance, Fe retention was > 0.60 at the beginning of batch one and drastically
244 decreased over the course of the NF, reaching negative values (Figure 3), that is, the permeate
245 concentration was higher than the concentration in the retentate. From batch two onwards, the
246 initial Fe retention was < 0.40 and showed a falling trend during NF (Figure 3). The mean Fe
247 retention over the entire NF stage was only $\sim 20\%$. Overall, the Sc over Fe selectivity (i.e. the ratio
248 of R_{Sc}/R_{Fe}) was exceptionally high, reaching a mean of 4.5, whereas the bench-scale test reached
249 a maximum of 2.7.¹⁰

250 Apart from Fe, U retention was remarkably low and constantly negative throughout the NF, except
251 for the very first recorded value in batch one. The extremely high U permeability was reflected in
252 an average retention of -0.97 and a yield of only 24% in the NF concentrate. This behaviour was
253 only matched by monovalent cations, such as Na^+ , reaching an average retention of -0.72 and a
254 final yield of 29% in the NF concentrate. The U retention found is in line with the results of Rem-
255 men et al.³ One explanation could be the speciation of U in chloride-rich acidic environments,
256 that is, the presence of monovalent or uncharged complexes. This finding was confirmed by EX-
257 AFS measurements showing the presence of chloro-uranyl complexes, such as $\text{UO}_2(\text{H}_2\text{O})_x\text{Cl}^+$
258 and $\text{UO}_2(\text{H}_2\text{O})_x\text{Cl}_2$, at HCl concentrations of $\geq 4 \text{ mol L}^{-1}$.³³ For future recovery of U from complex
259 streams, where co-extraction represents a challenge in SX, the aforementioned phenomenon in
260 NF could be leveraged as a U pre-separation step.

261 A steady increase in permeate flow during Sc concentration was observed from batch one to
262 batch five (Figure 3). Except for the first batch, the permeate flow started at its highest value and
263 declined as the feed concentration advanced. However, the permeate flux in the first batch started
264 low ($1.25 \pm 0.05 \text{ L m}^{-2} \text{ h}^{-1}$), subsequently increased ($2.5 \pm 0.1 \text{ L m}^{-2} \text{ h}^{-1}$ at 20% permeate recovery)
265 and then decreased again ($1.22 \pm 0.07 \text{ L m}^{-2} \text{ h}^{-1}$ at 60% permeate recovery) (Figure 3). This 'par-
266 abolic' behaviour was not previously observed in bench-scale tests. One explanation might be
267 the five times larger membrane area in the pilot trials, which would have required a longer swelling
268 time initially.³⁴

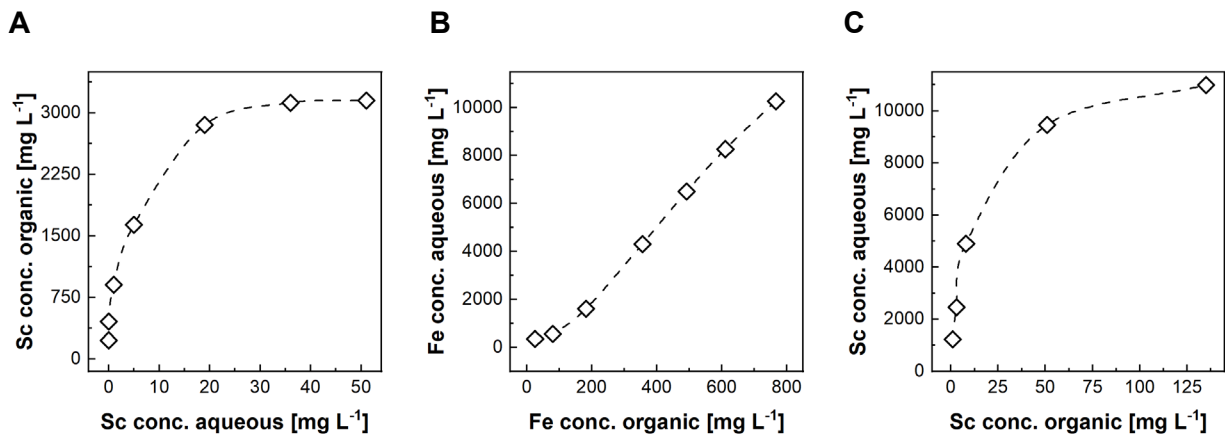
269 During the bench-scale tests, membranes were only used once for the concentration experi-
270 ments. As shown in this process, reusing was beneficial in terms of permeate flux and Sc selec-
271 tivity over several impurities, such as Fe, V or U (Figure 3). The behaviour is in agreement with
272 previous studies showing that acid soaking may result in higher permeability of polyethylene-
273 imine-coated thin film composite membranes.^{35,36} Although not disclosed, AMS patents suggest
274 a comparable active layer in the NanoPro A-3014 membrane.^{37,38} In addition, despite the higher
275 permeate flux in batches three to five, no higher element retention was observed (Figure 3), indi-
276 cating that the ion flux increased proportionally to the water flux (convective flow). Lopez et al.
277 observed a similar behaviour when testing NF for rare earth element recovery from acidic solu-
278 tions and interpreted it as a sign of increased pore size caused by degradation.³⁹ In contrast to

279 the aforementioned study, an especially acid-resistant NF membrane was used in our study to
280 withstand HCl exposure. Although partial membrane degradation cannot be excluded, the simi-
281 larity of element retentions and permeate fluxes in batches three to five indicates the NanoPro A-
282 3014's primary suitability for the application (Figure 3). Therefore, the membrane can be further
283 reused. Based on the results, longer membrane equilibration prior to NF should be considered for
284 future Sc recovery.

285 The production of 2.5-fold concentrated acid waste through NF took 31 h (310 h m^{-3}). The in-
286 crease in permeate flow rate (average batch one: $1.8 \text{ L m}^{-2} \text{ h}^{-1}$; average batch five: $4.7 \text{ L m}^{-2} \text{ h}^{-1}$)
287 resulted in decreased operating time with each batch. Furthermore, the energy consumption rate
288 was almost constant during the entire NF (1 kWh h^{-1}). Accordingly, the respective energy cost
289 decreased with each batch due to the accelerating filtration rate. The mean SEC for concentrate
290 production was 327 and 265 kWh m^{-3} , considering only the last three batches (both referring to
291 concentrate volume). The key to the high energy demand of NF was the low permeate flux (max.
292 $5.8 \text{ L m}^{-2} \text{ h}^{-1}$ at 35 bar TMP). The use of RO or NF with small membrane permeability has already
293 been reported (e.g. in the field of acid purification).⁴⁰ However, SEC needs to be optimised to
294 improve process profitability for future applications. In this process, highly permeable LbL mem-
295 branes could be of interest as soon as more stable products suitable for highly concentrated
296 streams become commercially available.³ The minimisation of the cross-flow rate could be an
297 option in the case of the NanoPro A-3014. A reduction is possible as long as permeate flux and
298 Sc retention are not impaired⁴¹ and no scaling occurs (unlikely at pH 1.5). Moreover, the energy
299 demand per membrane area can be decreased by further upscaling the system.⁴² For example,
300 a pump delivering 10 times the flow would consume proportionally more energy but could feed
301 an 8040 element that has 15 times the membrane area of a 2540 element.^{43–45} Consequently,
302 SEC could be cut by a third. Furthermore, a smaller spacer (31 mil instead of 46 mil) could in-
303 crease the membrane area per element, specifically by 25%, in the case of 8040 elements.⁴³
304 Finally, the implementation of energy recovery devices, such as Pelton turbines, could recover
305 30–40% of the total energy.^{46,47} These adjustments could result in 70% savings in SEC.

306 In summary, the pilot NF performed better than the bench scale, recovering more Sc with better
307 selectivity and demonstrating that membrane reuse does not only reduce investment costs but
308 also improves Sc selectivity and operating speed. The high SEC calls for membrane and system
309 optimisation, providing a starting point for future efforts.

310 **Solvent extraction**



311 **Figure 4:** Equilibrium diagrams for loading (A), scrubbing (B) and stripping (C) of Sc using 0.2 mol L⁻¹ D2EHPA with 0.05 mol L⁻¹
 312 N1923 in D80 kerosene at the bench scale.

313 **Table 2:** Average phase separation speed in each step of SX.

Process step	Separation Speed [m h ⁻¹]
Extraction	3.4
Scrubbing	2.6
Washing	14.8
Stripping	10.8
Conditioning	3.9

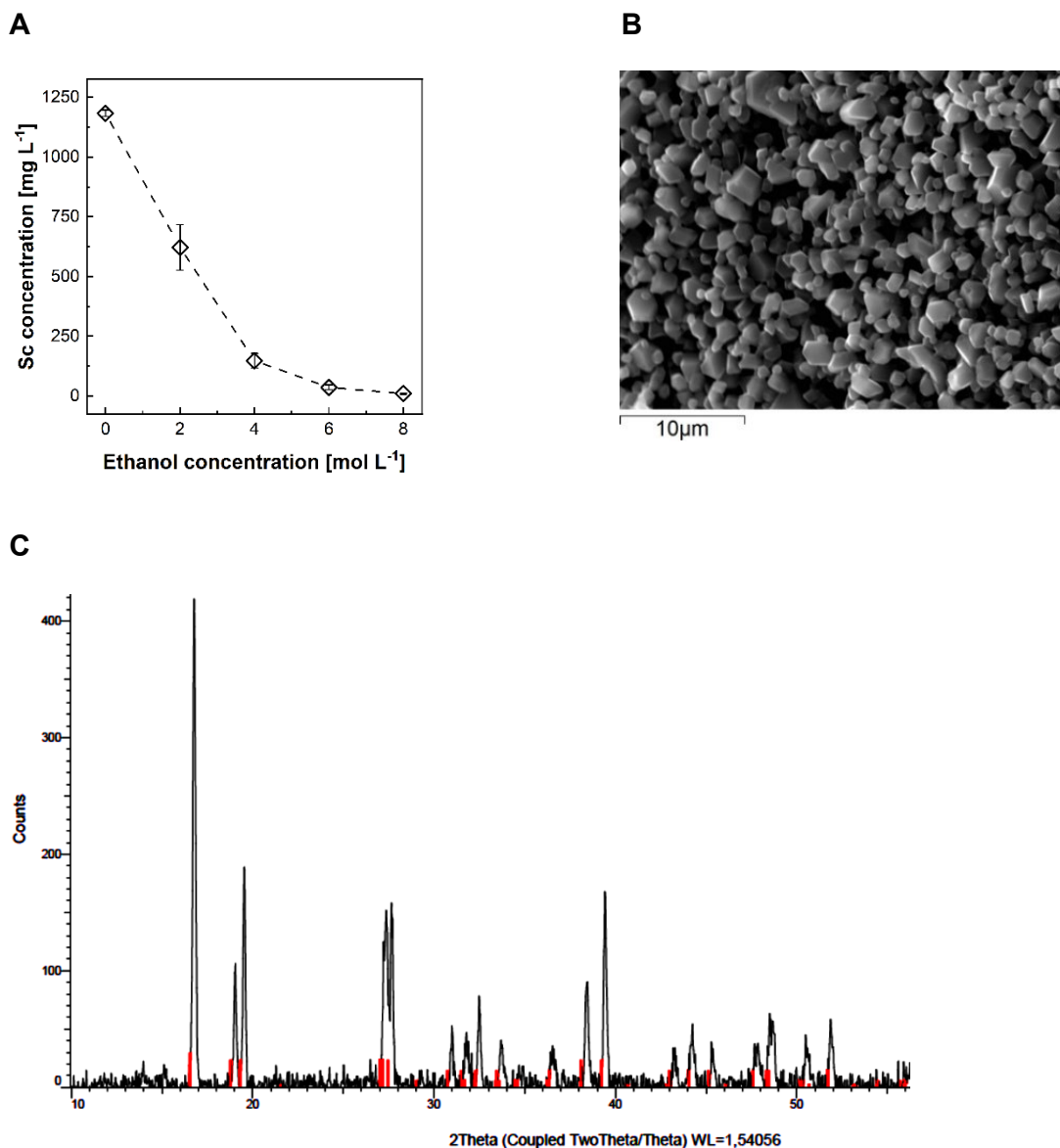
314
 315 As previously reported, a synergistic mixture of D2EHPA and N1923 reduces the co-extraction of
 316 impurities, such as V and Fe, in the SX circuit.¹⁰ Based on this, 0.2 mol L⁻¹ D2EHPA with 0.05 mol
 317 L⁻¹ N1923 in D80 kerosene was used as the organic solution for the pilot testing. The equilibria
 318 for Sc loading, scrubbing and stripping were determined on a bench scale prior to the pilot exper-
 319 iments (Figure 4). A maximum loading of 3 g L⁻¹ was observed during the laboratory investigations
 320 (Figure 4A). However, worse separation behaviour was observed beyond the Sc loading of
 321 1.5 g L⁻¹. The organic started foaming, slowing down phase separation due to high Sc loading,
 322 which ultimately prevented continuous processing at this loading level. Therefore, Sc loading was
 323 chosen between 0.5–0.7 g L⁻¹, eliminating phase separation issues and yielding fast separation.
 324 Based on the equilibrium loading diagram, full Sc loading required two stages of extraction (Figure
 325 4A).

326 In terms of scrubbing behaviour, using HCl (4 mol L⁻¹) in 3–4 scrubbing stages resulted in the
 327 effective removal of the co-extracted Fe from the loaded organic (Figure 4B). In addition, D2EHPA
 328 showed considerably higher affinity to Fe³⁺ than to Fe²⁺, wherefore the addition of Fe⁰ suppressed
 329 Fe co-extraction by reducing Fe³⁺.¹⁰ As such, Fe⁰ was added to the NF concentrate before the
 330 loading stage. The scrub liquor (i.e. spent HCl after scrubbing) was recycled into the loading feed
 331 solution to eliminate Sc losses and lower the solution pH, thereby suppressing Fe²⁺ co-extraction.

332 Investigations on Sc stripping equilibrium (Figure 4C) confirmed the effectiveness of NH_4F (3 mol
333 L^{-1}). Complete Sc stripping was achieved in most cases. However, the solubility limit of $(\text{NH}_4)_3\text{ScF}_6$
334 ($\sim 7.5 \text{ g L}^{-1}$)¹⁹ at Sc concentrations above 2 g L^{-1} was exceeded, leading to crystallisation. Since
335 solid precipitate could harm the SX process by forming cruds and inseparable phases, causing
336 organic losses, a final Sc concentration of $1.0\text{--}1.5 \text{ g L}^{-1}$ was targeted for the strip liquor. Based
337 on the equilibrium data, four stages of stripping were required for effective Sc stripping (Fig-
338 ure 4C).

339 The settling behaviour in each SX step was investigated, and the separation speeds of the aque-
340 ous and organic solutions were calculated (Table 2). In all cases, separation speeds exceeded 2
341 m h^{-1} , implying rapid, successful separations (Table 2). Moreover, both mixing modes (aqueous
342 or organic phase as the dispersant) were tested. However, no impact on separation behaviour
343 was observed. Generally, no phase separation problems occurred in the pilot SX tests.

344 The processing of the entire NF concentrate (100 L) lasted for 17 h. The pilot SX worked efficiently
345 with only minute Sc losses, reaching a yield of $\sim 98\%$ (three stages) and a tenfold increase of Sc
346 concentration in the strip liquor ($\sim 1.27 \pm 0.04 \text{ g L}^{-1}$; stream 18, Table 1). Impurities in the product
347 included V, Th, U and Fe (Table 1). Despite the removal of most Fe, minute amounts were still
348 present in the strip liquor, probably due to the spontaneous oxidation of Fe^{2+} to Fe^{3+} during the
349 continuous operation. To prevent this occurrence in the future, sealed mixer-separator units could
350 be used instead of running the SX in an open atmosphere. Although only traces of Th and U were
351 observed in the NF concentrate, they were almost inseparable from Sc in SX. Therefore, 75% of
352 U and 21% of Th ended up in the strip liquor. Notably, the mass balance for Th after stripping did
353 not add up, and 67% of the total extracted Th was neither measured in the stripped organic nor
354 in the strip liquor. Insoluble Th complexes possibly formed after NH_4F addition and precipitated
355 without being noticed in the pilot unit. In the case of V, co-extraction was well suppressed by the
356 use of N1923 as co-extractant, leading to only 6% co-extraction (Table 1). In the scrubbing stage,
357 90% of the extracted V was removed (Table 1). The 0.3% (i.e. 0.6 g) initial V that was eventually
358 stripped still made it a major impurity in the strip liquor due to its high starting concentration (Table
359 1). In total, approximately 90% Sc purity was reached, which was below par with the previously
360 reported bench scale result of 97%.¹⁰ Although the entire NF concentrate was processed, the SX
361 process had probably not yet reached its equilibrium. Supposedly, higher purities can be attained
362 in a longer continuous operation. During the pilot trials, the purity levels in the samples collected
363 increased as the SX process continued.



365 **Figure 5:** Solution concentration profile for Sc (A), SEM micrograph of the solid obtained at 8 mol L⁻¹ ethanol (B) and XRD pattern of
 366 the solid product obtained at 8 mol L⁻¹ (C). The red lines are the reference pattern for (NH₄)₃ScF₆ of monoclinic-structure PDF card
 367 00-040-0595 (C).

368
 369 Sc crystallisation started quickly after the addition of ethanol to the strip liquor. The amount of
 370 precipitated Sc asymptotically approached a scandium recovery of > 95 % with increasing ethanol
 371 concentration (Figure 5A). A concentration of 8 mol L⁻¹ appeared optimal to maximise Sc recovery
 372 with a yield of 96% (Table 1).

373 After instantaneous antisolvent addition (8 mol L⁻¹), discrete, regular-shaped crystals with an av-
 374 erage size of approximately 1–2 μm were obtained, as seen in the SEM image (Figure 5B). The
 375 mean size and size distribution of the crystal product can be controlled by seeding and supersat-
 376 uration control.²⁰ Powder XRD measurements identified the obtained solids as predominantly
 377 (NH₄)₃ScF₆ (PDF 00-040-0595; Figure 5C). The peaks of other ammonium metal fluorides, such

378 as Zr, V, Al or Fe, which were present in the strip liquor could not be detected. This could indicate
379 low concentrations in the solid material but may also be attributed to similar peak positions of
380 most ammonium metal fluorides.

381 Element concentrations were also measured in the strip liquor before and after ASC with 8 mol
382 L⁻¹ ethanol (Table 1). Based on the results, the solid product's purity was determined to be 93.5%
383 on a metal basis or 95.1% on the basis of ammonium metal fluorides (Table S1; assuming the
384 formation of ammonium metal fluoride complexes for all impurities). Impurities could be incorpo-
385 rated into crystal lattices or adhere to the crystal surfaces without actually precipitating as ammo-
386 nium metal fluorides. As reported previously, Ti tends to remain solubilised, most likely due to its
387 stable titanyl ion (TiO²⁺) in the solution.¹⁸ Similar to their abundance in the strip liquor, the major
388 impurities found in the solid product were V, Th and U (ordered by mass fraction; Table 1). Fur-
389 thermore, minute amounts of Al and Zr are present in the solid (Table 1). Comparable to SX, the
390 product purity after ASC was below par compared with the previously reported purities of ca
391 99%.¹⁷ As previously described, SX was probably further away from its equilibrium than during
392 the bench scale tests, which also negatively affected the downstream ASC. Hence, the easiest
393 solution would be to further optimise Sc selectivity upstream to ASC. This result could also be
394 partly due to the lower initial Sc concentration in the strip liquor than previously reported.¹⁷ None-
395 theless, crystallisation in more stages, starting with a lower amount of antisolvent and better con-
396 trol of the supersaturation during crystallisation, could help increase the purity, potentially at the
397 cost of total yield.^{18,20,48} Moreover, purification of the product could be achieved through a combi-
398 nation of SX and ion exchange.^{23,49}

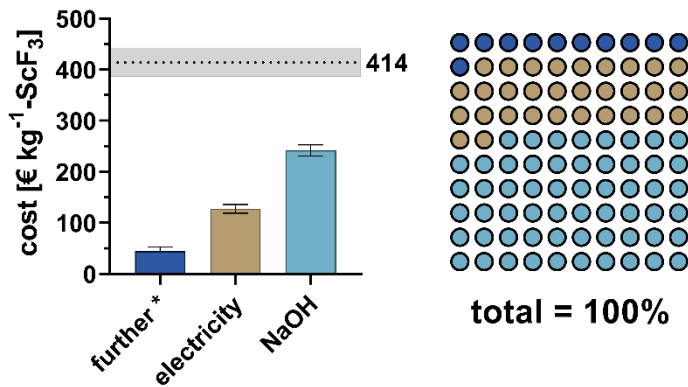
399 In terms of ASC process design, the required ethanol amount of 0.88 L per litre strip liquor ap-
400 peared high. However, the spent ethanol can be distilled and reused in ASC without deterioration
401 of precipitation efficiency. In a previous study, methanol and ethanol recovered through simple
402 distillation with alcohol purities of 75–85% (v/v) showed Sc recovery efficiencies > 97% when
403 reused in ASC.⁵⁰ Furthermore, after antisolvent distillation, the spent aqueous solution, which was
404 partially depleted in NH₄F, can be reused in the SX stripping stage with adequate make-up (Fig-
405 ure 1).

406 **Process flows and production cost assessment**

407 **Table 3:** Energy and material flows and costs to produce 1 kg of ScF₃.

Description		AF	SX	ASC	CAL	Total	Sum energy and material costs [€]
Acid waste	[kg]	13'198				13'198	-
Ethanol	[kg]			25		25	6-20
HCl 33%	[kg]		42			42	4-5
NaOH 30%	[kg]	3'160				3'160	230-253
NH ₄ F (3 mol L ⁻¹)	[kg]		36			36	4
Fe powder	[kg]		5.3			5.3	10-12
Water	[kg]		69			69	0.01
Electricity	[kWh]	2'426	3.7	1.1	0.9	2'432	119-136
Heat	[kWh]			576		576	12
Waste	[kg]	13'198	4'012	42		17'252	-
Total costs	[€]	350-389	18-22	18-31	0.04-0.05	386-442	386-442

408



409

410 **Figure 6:** Costs for ScF₃ production. Bars indicate maximal/minimal assumptions for prices. Note that etha-
 411 nol, HCl, NH₄F, Fe powder, water and heat combined contributed little (11%) to the overall cost and are
 412 summarised as 'further'.

413 The developed process was benchmarked based on the production of 1 kg ScF₃ as the market-
 414 able product closest to (NH₄)₃ScF₆. As previously reported, (NH₄)₃ScF₆ can be easily converted
 415 into ScF₃ by calcination.⁵¹ Following previous studies, the conversion of 2.1 kg (NH₄)₃ScF₆ into 1
 416 kg ScF₃ was considered with an input of 0.9 kWh electricity (Table 3).⁵²⁻⁵⁴ Furthermore, for AF,
 417 filter materials, such as the organic phase in SX, were assumed to be fully reusable. For SX and
 418 ASC, 90% recyclability of NH₄F solution and antisolvent was assumed, respectively. The under-
 419 lying prices used for assessment are given in SI (Table S2).

420 The total input for the production of 1 kg ScF₃ from ~13,000 kg AW totalled to ~3,400 kg of mate-
421 rials and ~3,000 kWh of energy consumption (Table 3). The generated waste was ~17,300 kg.
422 Given that the waste is a mix of hydroxides, it could be disposed of similarly to the TiO₂ plant
423 waste treatment.

424 The total material and energy costs to produce 1 kg ScF₃ were ~414 ± 28 € (Table 3, Figure 6).
425 United States Geological Survey (2022) reported a price (1–5 g lot size) of US\$216,000 (~216,000
426 €) per kilogram of ScF₃, which is assumed to be very high.⁵ Prices on online portals (e.g.
427 alibaba.com) range between ~721–1546 € kg⁻¹ of ScF₃ (99–99.99% purity; Table S2). Hence, the
428 production costs for ScF₃ determined in this study were considerably lower than the market prices
429 reported.

430 Among all the process inputs, NaOH had the highest cost share (~58%; Figure 6), followed by
431 electricity consumption (~31%; Figure 6). All further inputs contributed only 11% to the total costs
432 (Figure 6). On the process level, the initial AF step had the major cost share (~89%; Table 3).
433 Therefore, process optimisation should target the AF stage first. As previously described, a high
434 optimisation potential for the energy consumption of AF is expected (savings of 95% for UF and
435 70% for NF). This could reduce the energy consumption by ~2000 kWh kg⁻¹ of ScF₃, lowering the
436 production cost by 25% or 110 € kg⁻¹. The primary cost driver would still be neutralising with
437 NaOH. The neutralisation, although assigned to the AF stage in this study, is already a part of
438 waste treatment in TiO₂ production. Hence, the actual cost of pH adjustment in AF should be
439 calculated as the difference between the cost for neutralisation with NaOH or with lime/limestone,
440 similar to the current practice. Using CaO/CaCO₃ would not be an option in AF, as Ca²⁺ shows
441 considerably higher retention than Na⁺ in NF, thereby increasing the osmotic pressure and dete-
442 riorating filtration performance. Kapil et al. compared the neutralisation efficiency for different
443 chemicals, revealing a 10% lower consumption of CaCO₃ compared with NaOH for reaching the
444 same pH.⁵⁵ Thus, considering a slightly lower price per kilogram for limestone than for caustic
445 soda, a treatment with NaOH is expected to cost roughly 20% more (Table S3). This means that
446 the existing TiO₂ production already covers 80% of the neutralisation costs (i.e. ~200 € kg⁻¹ ScF₃)
447 previously allocated to AF. Therefore, the additional neutralisation cost during AF is estimated to
448 be 50 ± 5 € kg⁻¹ ScF₃.

449 In summary, the entire AF would realistically cost around 70 ± 30 € kg⁻¹ ScF₃, which is approxi-
450 mately 80% lower than the current pilot operation. In this scenario, a total material and energy
451 cost for ScF₃ of 120 ± 40 € kg⁻¹ is conceivable. The overall process yield (43%, nine stages) could
452 be improved, bearing the potential to cut the production cost in half. The Sc losses during the
453 initial S/L separation (MF and UF) could be easily minimised by exchanging bag filtration with a
454 filter press similar to that used in TiO₂ production.

455

456 **Conclusion**

457 This study demonstrated the feasibility of combining AF techniques, SX and ASC to obtain 95%
458 pure $(\text{NH}_4)_3\text{ScF}_6$ as a close-to-market Sc product from a real TiO_2 acid waste. Major challenges
459 during AF included the low filtration rates because of small particle size and hygroscopicity of the
460 precipitated hydroxides and the osmotic pressure of the feed. NF improved with the progression
461 of the pilot tests, yielding higher permeate flux and Sc selectivity, which were interpreted as ben-
462 efits of membrane equilibration. Overall, the process volume was reduced through NF by 60%,
463 with 87% Sc yield and depletion of impurities such as Fe, V and U.

464 During pilot SX, high separation efficiency for Sc was observed with the previously published
465 process.¹⁰ Phase separation worked rapidly, and tertiary phases did not occur. However, the
466 achieved purity still left room for improvement, calling for longer test runs that allow better process
467 equilibration and a closed system to minimise spontaneous Fe oxidation. In total, a tenfold con-
468 centrated Sc liquor (98% yield, three stages) was produced, with minimal co-extraction of com-
469 peting elements such as Fe or V.

470 Using strip liquor, the ASC tests indicated the addition of 0.88 v/v ethanol as the best option,
471 delivering the highest Sc yield (96%).

472 The overall process has the potential to produce ScF_3 at competitive market prices from a Euro-
473 pean secondary source. Thus, the combination of AF-SX-ASC could boost the supply of Sc, mit-
474 igating possible policy-induced shortages in the future.

475 **Supporting Information**

476 The Supporting Information is available free of charge at
477 <https://pubs.acs.org/doi/xx.xxxx/acssuschemeng.xxxxxxx>.

478 Equations used to calculate the advanced filtration performance, overview of the pilot plants (AF
479 and SX), breakdown of elemental concentrations used for purity calculations, and overview of
480 specific costs used for the production cost assessment.

481 **Acknowledgements**

482 This project has received funding from the European Union's Horizon 2020 research and innova-
483 tion programme under Grant Agreement No. 730105 (SCALE: www.scale-project.eu/). This work
484 was supported by the Swiss State Secretariat for Education, Research and Innovation (SERI)
485 under Contract No. 16.0155. The opinions expressed and arguments employed herein do not
486 necessarily reflect the official views of the Swiss government. We acknowledge the University of
487 Basel for its continuing support. We also thank Kirsten Remmen for her assistance during the
488 completion of this study. The table of contents/abstract graphic was created with BioRender.com.

489 **References**

- 490 (1) European Commission. *Critical Raw Materials Resilience: Charting a Path towards Greater*
491 *Security and Sustainability:COM/2020/474 final, 2020.*
- 492 (2) European Commission. *on the 2017 list of Critical Raw Materials for the EU:COM(2017) 490*
493 *final, Sep 13, 2017.*
- 494 (3) Remmen, K.; Schäfer, R.; Hedwig, S.; Wintgens, T.; Wessling, M.; Lenz, M. Layer-by-layer
495 membrane modification allows scandium recovery by nanofiltration. *Environ. Sci.: Water Res.*
496 *Technol.* **2019**, *5* (10), 1683–1688. DOI: 10.1039/C9EW00509A.
- 497 (4) Ukai, K.; Yokoyama, M.; Shimano, J.; Mizutani, Y.; Yamamoto, O. An Overview of Scandia
498 Stabilized Zirconia Electrolyte Development for SOFC Application. In *Ceramic Materials and*
499 *Components for Energy and Environmental Applications*; Jiang, D., Zeng, Y., Singh, M., Hein-
500 rich, J., Eds.; Ceramic Transactions Series; John Wiley & Sons, Inc, 2010; pp 185–190. DOI:
501 10.1002/9780470640845.ch25.
- 502 (5) Cordier, D. J. *USGS Mineral Commodity Summary: Scandium, 2022.*
- 503 (6) Blengini, G. A.; Latunussa, C. E. L.; Eynard, U.; Torres de Matos, C.; Wittmer, D.; Georgitzi-
504 kis, K.; Pavel, C.; Carrara, S.; Mancini, L.; Unguru, M.; Blagoeva, D.; Mathieux, F.; Pennington,
505 D. *Study on the EU's list of critical raw materials (2020)*; Publications Office of the European
506 Union, 2020.
- 507 (7) Gambogi, J. Rare Earths. In *Metals and minerals: U.S. Geological Survey Minerals Year-*
508 *book - 2016*; U.S. Geological Survey, Ed.; Minerals Yearbook, I; U.S. Government Publishing
509 Office, 2018.
- 510 (8) Perks, C.; Mudd, G. Titanium, zirconium resources and production: A state of the art litera-
511 ture review. *Ore Geol. Rev.* **2019**, *107*, 629–646. DOI: 10.1016/j.oregeorev.2019.02.025.
- 512 (9) Gázquez, M. J.; Bolívar, J. P.; Garcia-Tenorio, R.; Vaca, F. A Review of the Production Cy-
513 cle of Titanium Dioxide Pigment. *MSA* **2014**, *05* (07), 441–458. DOI: 10.4236/msa.2014.57048.
- 514 (10) Hedwig, S.; Yagmurlu, B.; Huang, D.; Arx, O. von; Dittrich, C.; Constable, E. C.; Friedrich,
515 B.; Lenz, M. Nanofiltration-Enhanced Solvent Extraction of Scandium from TiO₂ Acid Waste.
516 *ACS Sustainable Chem. Eng.* **2022**, *10* (18), 6063–6071. DOI:
517 10.1021/acssuschemeng.2c01056.
- 518 (11) Vickery, R. C. The extraction and purification of scandium. *J. Chem. Soc.* **1955**, 245. DOI:
519 10.1039/JR9550000245.
- 520 (12) Wang, W.; Pranolo, Y.; Cheng, C. Y. Metallurgical processes for scandium recovery from
521 various resources: A review. *Hydrometallurgy* **2011**, *108* (1-2), 100–108. DOI: 10.1016/j.hy-
522 dromet.2011.03.001.
- 523 (13) Shaoquan, X.; Suqing, L. Review of the extractive metallurgy of scandium in China (1978–
524 1991). *Hydrometallurgy* **1996**, *42* (3), 337–343. DOI: 10.1016/0304-386X(95)00086-V.

- 525 (14) Martinez, A. M.; Osen, K. S.; Gudbrandsen, H.; Sommerseth, C.; Wang, Z.; Darell, O. Di-
526 rect Method for Producing Scandium Metal and Scandium-Aluminium Intermetallic Compounds
527 from the Oxides. In *Light Metals 2018*; Martin, O., Ed.; The minerals, metals & materials series;
528 Springer International Publishing, 2018; pp 1559–1564. DOI: 10.1007/978-3-319-72284-9_203.
- 529 (15) Kulikov, B. P.; Baranov, V. N.; Bezrukikh, A. I.; Deev, V. B.; Motkov, M. M. Preparation of
530 Aluminum-Scandium Master Alloys by Aluminothermal Reduction of Scandium Fluoride Ex-
531 tracted from Sc₂O₃. *Metallurgist* **2018**, *61* (11-12), 1115–1121. DOI: 10.1007/s11015-018-
532 0614-1.
- 533 (16) Harata, M.; Nakamura, T.; Yakushiji, H.; Okabe, T. H. Production of scandium and Al–Sc
534 alloy by metallothermic reduction. *Mineral Processing and Extractive Metallurgy* **2008**, *117* (2),
535 95–99. DOI: 10.1179/174328508X290876.
- 536 (17) Peters, E. M.; Kaya, Ş.; Dittrich, C.; Forsberg, K. Recovery of Scandium by Crystallization
537 Techniques. *J. Sustain. Metall.* **2019**, *5* (1), 48–56. DOI: 10.1007/s40831-019-00210-4.
- 538 (18) Peters, E. M.; Dittrich, C.; Yagmurlu, B.; Forsberg, K. Co-precipitation of Impurity (Ti, Fe,
539 Al, Zr, U, Th) Phases During the Recovery of (NH₄)₃ScF₆ from Strip Liquors by Anti-solvent
540 Crystallization. In *Rare Metal Technology 2020*; Azimi, G., Forsberg, K., Ouchi, T., Kim, H.,
541 Alam, S., Baba, A. A., Eds.; The minerals, metals & materials series; Springer International Pub-
542 lishing, 2020; pp 177–189. DOI: 10.1007/978-3-030-36758-9_17.
- 543 (19) Peters, E. M.; Svärd, M.; Forsberg, K. Phase equilibria of ammonium scandium fluoride
544 phases in aqueous alcohol mixtures for metal recovery by anti-solvent crystallization. *Separation and Purification Technology* **2020**, *252*, 117449. DOI: 10.1016/j.seppur.2020.117449.
- 546 (20) Peters, E. M.; Svärd, M.; Forsberg, K. Impact of process parameters on product size and
547 morphology in hydrometallurgical antisolvent crystallization. *CrystEngComm* **2022**, *24* (15),
548 2851–2866. DOI: 10.1039/D2CE00050D.
- 549 (21) Zhou, J.; Ma, S.; Chen, Y.; Ning, S.; Wei, Y.; Fujita, T. Recovery of scandium from red
550 mud by leaching with titanium white waste acid and solvent extraction with P204. *Hydrometal-*
551 *lurgy* **2021**, *204*, 105724. DOI: 10.1016/j.hydromet.2021.105724.
- 552 (22) Chen, Y.; Ma, S.; Ning, S.; Zhong, Y.; Wang, X.; Fujita, T.; Wei, Y. Highly efficient recovery
553 and purification of scandium from the waste sulfuric acid solution from titanium dioxide produc-
554 tion by solvent extraction. *Journal of Environmental Chemical Engineering* **2021**, *9* (5), 106226.
555 DOI: 10.1016/j.jece.2021.106226.
- 556 (23) Zhou, J.; Ning, S.; Meng, J.; Zhang, S.; Zhang, W.; Wang, S.; Chen, Y.; Wang, X.; Wei, Y.
557 Purification of scandium from concentrate generated from titanium pigments production waste.
558 *Journal of Rare Earths* **2020**. DOI: 10.1016/j.jre.2020.02.008.
- 559 (24) Zhou, J.; Yu, Q.; Huang, Y.; Meng, J.; Chen, Y.; Ning, S.; Wang, X.; Wei, Y.; Yin, X.; Liang,
560 J. Recovery of scandium from white waste acid generated from the titanium sulphate process

561 using solvent extraction with TRPO. *Hydrometallurgy* **2020**, *195*, 105398. DOI: 10.1016/j.hy-
562 dromet.2020.105398.

563 (25) Howe, K. J.; Marwah, A.; Chiu, K.-P.; Adham, S. S. Effect of membrane configuration on
564 bench-scale MF and UF fouling experiments. *Water research* **2007**, *41* (17), 3842–3849. DOI:
565 10.1016/j.watres.2007.05.025. Published Online: May. 23, 2007.

566 (26) Gasper, H., Ed. *Handbuch der industriellen Fest/Flüssig-Filtration*, 2., vollst. überarb. und
567 stark erw. Aufl.; Wiley-VCH, 2000.

568 (27) Eaton Corporation. Considerations in bag filtration. *Filtration + Separation* **2020**, *57* (4),
569 20–23. DOI: 10.1016/S0015-1882(20)30234-2.

570 (28) Meschke, K.; Herdegen, V.; Aibel, T.; Janneck, E.; Repke, J.-U. Treatment of opencast
571 lignite mining induced acid mine drainage (AMD) using a rotating microfiltration system. *Journal*
572 *of Environmental Chemical Engineering* **2015**, *3* (4), 2848–2856. DOI:
573 10.1016/j.jece.2015.10.013.

574 (29) Chamberland, J.; Mercier-Bouchard, D.; Dussault-Chouinard, I.; Benoit, S.; Doyen, A.; Brit-
575 ten, M.; Pouliot, Y. On the Use of Ultrafiltration or Microfiltration Polymeric Spiral-Wound Mem-
576 branes for Cheesemilk Standardization: Impact on Process Efficiency. *Foods (Basel, Switzer-*
577 *land)* **2019**, *8* (6). DOI: 10.3390/foods8060198. Published Online: Jun. 8, 2019.

578 (30) Vatai, G. N.; Krstic, D. M.; Koris, A. K.; Gáspár, I. L.; Tekic, M. N. Ultrafiltration of oil-in-wa-
579 ter emulsion: Comparison of ceramic and polymeric membranes. *Desalination and Water Treat-*
580 *ment* **2009**, *3* (1-3), 162–168. DOI: 10.5004/dwt.2009.455.

581 (31) Crocker, W. A. Evaluation of Sludge Dewatering Alternatives at a Metallurgical Refinery.
582 *Journal of the Water Pollution Control Federation* **1982**, *54* (10), 1417–1424.
583 <https://www.jstor.org/stable/25041715>

584 (32) Montgomery Watson Harza. *MWH's water treatment: Principles and design*, 3. ed.; John
585 Wiley & Sons, 2012.

586 (33) Allen, P. G.; Bucher, J. J.; Shuh, D. K.; Edelstein, N. M.; Reich, T. Investigation of Aquo
587 and Chloro Complexes of UO(2)(2+), NpO(2)(+), Np(4+), and Pu(3+) by X-ray Absorption Fine
588 Structure Spectroscopy. *Inorganic chemistry* **1997**, *36* (21), 4676–4683. DOI:
589 10.1021/ic970502m.

590 (34) Lavania, J.; Rastogi, N. K.; Balaraman, M.; Rangaswamy, S. Nonlinear Flux-Pressure Be-
591 havior of Solvent Permeation through a Hydrophobic Nanofiltration Membrane. *ACS omega*
592 **2021**, *6* (41), 27052–27061. DOI: 10.1021/acsomega.1c03624. Published Online: Oct. 6, 2021.

593 (35) Zhang, Y.; Wan, Y.; Li, Y.; Pan, G.; Yu, H.; Du, W.; Shi, H.; Wu, C.; Liu, Y. Thin-film com-
594 posite nanofiltration membrane based on polyurea for extreme pH condition. *Journal of Mem-*
595 *brane Science* **2021**, *635*, 119472. DOI: 10.1016/j.memsci.2021.119472.

- 596 (36) Bargeman, G. Recent developments in the preparation of improved nanofiltration mem-
597 branes for extreme pH conditions. *Separation and Purification Technology* **2021**, *279*, 119725.
598 DOI: 10.1016/j.seppur.2021.119725.
- 599 (37) Perry, M.; Ginzburg, V.; Ginzburg, B.; Lapido, P. Solvent And Acid Stable Membranes,
600 Methods Of Manufacture Thereof And Methods Of Use Thereof Inter Alia For Separating Metal
601 Ions From Liquid Process Streams. EP20100731115 20100113.
- 602 (38) Lee, K. P.; Zheng, J.; Bargeman, G.; Kemperman, A. J.; Benes, N. E. pH stable thin film
603 composite polyamine nanofiltration membranes by interfacial polymerisation. *Journal of Mem-*
604 *brane Science* **2015**, *478*, 75–84. DOI: 10.1016/j.memsci.2014.12.045.
- 605 (39) López, J.; Reig, M.; Gibert, O.; Torres, E.; Ayora, C.; Cortina, J. L. Application of nanofiltra-
606 tion for acidic waters containing rare earth elements: Influence of transition elements, acidity
607 and membrane stability. *Desalination* **2018**, *430*, 33–44. DOI: 10.1016/j.desal.2017.12.033.
- 608 (40) González, M. P.; Navarro, R.; Saucedo, I.; Avila, M.; Revilla, J.; Bouchard, C. Purification
609 of phosphoric acid solutions by reverse osmosis and nanofiltration. *Desalination* **2002**, *147* (1-
610 3), 315–320. DOI: 10.1016/S0011-9164(02)00558-1.
- 611 (41) Roy, Y.; Sharqawy, M. H.; Lienhard, J. H. Modeling of flat-sheet and spiral-wound nanofil-
612 tration configurations and its application in seawater nanofiltration. *Journal of Membrane Sci-*
613 *ence* **2015**, *493*, 360–372. DOI: 10.1016/j.memsci.2015.06.030.
- 614 (42) Okamoto, Y.; Lienhard, J. H. How RO membrane permeability and other performance fac-
615 tors affect process cost and energy use: A review. *Desalination* **2019**, *470*, 114064. DOI:
616 10.1016/j.desal.2019.07.004.
- 617 (43) AMS Technologies Ltd. *Datasheet AMS NanoPro A-3014*. [http://www.amsmembrane.com/
618 images/Data_sheets/3.3/AMS_NanoPro_A-3014_v.3.3_2020-06-18.pdf](http://www.amsmembrane.com/images/Data_sheets/3.3/AMS_NanoPro_A-3014_v.3.3_2020-06-18.pdf), **2022**.
- 619 (44) Wanner Engineering, Inc. *G03 Series Datasheet*. [https://www.hydra-cell.com/ltr2/ac-
620 cess.php?file=pdf/G03-Datasheet.pdf](https://www.hydra-cell.com/ltr2/access.php?file=pdf/G03-Datasheet.pdf), **2021**.
- 621 (45) Wanner Engineering, Inc. *G35 Series Datasheet*. [https://www.hydra-cell.com/ltr2/ac-
622 cess.php?file=pdf/G35-Datasheet.pdf](https://www.hydra-cell.com/ltr2/access.php?file=pdf/G35-Datasheet.pdf), **2021**.
- 623 (46) Wilson, W.; Gruendisch, A.; Calder-Potts, I. The use of pelton wheel turbines for energy
624 recovery in reverse osmosis systems. *Desalination* **1987**, *65*, 231–240. DOI: 10.1016/0011-
625 9164(87)90136-6.
- 626 (47) Gude, V. G. Energy consumption and recovery in reverse osmosis. *Desalination and Wa-*
627 *ter Treatment* **2011**, *36* (1-3), 239–260. DOI: 10.5004/dwt.2011.2534.
- 628 (48) Demirel, H. S.; Svärd, M.; Uysal, D.; Doğan, Ö. M.; Uysal, B. Z.; Forsberg, K. Antisolvent
629 crystallization of battery grade nickel sulphate hydrate in the processing of lateritic ores. *Sepa-*
630 *ration and Purification Technology* **2022**, *286*, 120473. DOI: 10.1016/j.seppur.2022.120473.
- 631 (49) Chen, Y.; Ning, S.; Zhong, Y.; Li, Z.; Wang, J.; Chen, L.; Yin, X.; Fujita, T.; Wei, Y. Study
632 on highly efficient separation of zirconium from scandium with TODGA-modified macroporous

633 silica-polymer based resin. *Separation and Purification Technology* **2023**, *305*, 122499. DOI:
634 10.1016/j.seppur.2022.122499.

635 (50) Peters, E. M.; Kaya, Ş.; Svärd, M.; Forsberg, K. *Recovery of alcohol after anti-solvent pre-*
636 *cipitation of (NH₄)₃ScF₆ from NH₄F strip liquors*; IMPC 2020: XXX International Mineral Pro-
637 cessing Congress, 2021.

638 (51) Kaya, Ş.; Peters, E.; Forsberg, K.; Dittrich, C.; Stopic, S.; Friedrich, B. Scandium Recovery
639 from an Ammonium Fluoride Strip Liquor by Anti-Solvent Crystallization. *Metals* **2018**, *8* (10),
640 767. DOI: 10.3390/met8100767.

641 (52) Lindsay, S. J. *Light Metals 2011*; Springer International Publishing, 2016. DOI:
642 10.1007/978-3-319-48160-9.

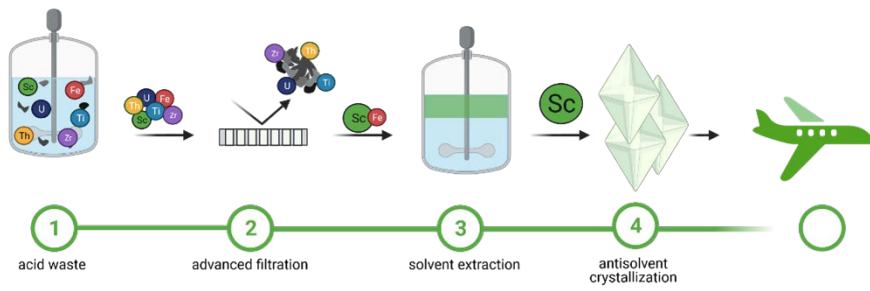
643 (53) Profaiser, A.; Saw, W.; Nathan, G. J.; Ingenhoven, P. Bottom-Up Estimates of the Cost of
644 Supplying High-Temperature Industrial Process Heat from Intermittent Renewable Electricity
645 and Thermal Energy Storage in Australia. *Processes* **2022**, *10* (6), 1070. DOI:
646 10.3390/pr10061070.

647 (54) Krähenbühl, M.; Etter, B.; Udert, K. M. Pretreated magnesite as a source of low-cost mag-
648 nesium for producing struvite from urine in Nepal. *The Science of the total environment* **2016**,
649 *542* (Pt B), 1155–1161. DOI: 10.1016/j.scitotenv.2015.08.060. Published Online: Oct. 21, 2015.

650 (55) Kapil, N.; Bhattacharyya, K. G. A comparison of neutralization efficiency of chemicals with
651 respect to acidic Kopili River water. *Appl Water Sci* **2017**, *7* (5), 2209–2214. DOI:
652 10.1007/s13201-016-0391-6.

653

654 **For Table of Contents Use Only**



655

656

657

Synopsis: Piloted scandium separation from TiO_2 production waste using a combination of advanced filtration techniques, solvent extraction and antisolvent crystallisation.